

Electronic supplementary information

High-Sensitivity Microliter Blood Pressure Sensors Based on Patterned Micro-nanostructure Arrays

Nianzuo Yu,^a Yongshun Liu,^{*,b} Bai Ji,^c Shuli Wang,^a YunYun Chen,^c Tianmeng Sun,^d Junhu Zhang,^{*,a} and Bai Yang^a

^aState Key Laboratory of Supramolecular Structure and Materials, College of Chemistry, Jilin University, 130012, P. R. China

^bState Key Laboratory of Applied Optics, Changchun Institute of Optics, Fine Mechanics and Physics (CIOMP), Chinese Academy of Sciences, 130033, P. R. China

^c Department of Hepatobiliary and Pancreatic Surgery, the First Hospital, Jilin University, P. R. China

^d Institute of Immunology, International Center of Future Science, the First Hospital, Jilin University, P. R. China

*Corresponding author. E-mail: zjh@jlu.edu.cn

This file includes:

Fig. S1. The diagram and surface wettability of the LPS.

Fig. S2. The filling process of water in the LPS with incremental metering microchannels.

Fig. S3. The filling behaviors of water in the LPS with high, shallow, distant and closed metering microchannels.

Fig. S4. The filling behaviors of water in the LPS with wider metering microchannels and narrow outlets.

Fig. S5. The stability, response time and required liquid volume of the LPS.

Fig. S6. The LPS for sensing the applied pressure of wide surface tension ranges and multiphase liquids

Fig. S7. The diagram of the reservoir and cross-sectional of the LPS for sensing the applied pressure of liquids with extremely low surface tension and its measurement process.

Fig. S8. The filling behaviors of water in the metering microchannels when the widths of the fluidic microchannels are 100 μm and 300 μm .

Fig. S9. Optical microscopy images of the LPS for sensing the simulative central venous pressure and systolic blood pressure.

Legends for movies S1 to S2

Other Supplementary Material for this manuscript includes the following:

Video S1. (.mp4 format). The filling behavior of water in the LPS when the applied pressure of inlet is 130.0 mbar.

Video S2. (.mp4 format). Detecting the arterial blood pressure of mouse by the LPS.

Experimental Section

Materials. Silicon (Si) substrates were cleaned by immersion in piranha solution (7:3 concentrated H_2SO_4 /30% H_2O_2) for 2 h at 140 °C to create a hydrophilic surface. A photoresist (BP218-45s positive photoresist) was purchased from Kempur Microelectronics. A Sylgard 184 elastomer base and a curing agent for poly(dimethylsiloxane) were purchased from Dow Corning (Midland, MI). Poly(diallyldimethylammonium chloride) (PDDA), nitroglycerin, adrenaline, acetyl choline, Trichloro(1H,1H,2H,2H-perfluorooctyl)silane (PFS) were purchased from Aldrich. Pentobarbital sodium, saline, syringe needle, anticoagulation rat, horse and newborn bovine bloods were purchased from Solarbio, and the experimental blood sample was originated from the same bovine. Bull serum albumin (BSA) was purchased from SIGMA. Absolute ethanol, acetone, n-hexadecane and octadecene were used as received. Milli-Q water ($18.2 \text{ M}\Omega \text{ cm}^{-1}$) was used in all experiments.

Device Fabrication. Fabrication of the hydrophobic silicon micro-nanostructures substrates were conducted as reported earlier. The Si microstripes were fabricated by traditional lithography and RIE etching techniques. To fabricate nanopillars on Si microstripe surfaces, we used gold nanoparticles (Au NPs) as etching masks. The Au NPs have negative charges, and they can absorb to surfaces with positive charges by electrostatic interaction. Before absorption of Au NPs, Si stripes were treated by oxygen plasma and absorbed one layer of poly(diallyldimethylammonium chloride) (PDDA). Then, the Au NPs absorbed to the Si stripes covered by one layer of PDDA. After 3 h of absorption, the surfaces were rinsed by deionized water. Then, the RIE process was performed on the Au NP-absorbed Si stripes. Before etching Si, the exposed PDDA layer was removed by oxygen plasma for 2 min (RF = 60 W, ICP = 0 W, and total pressure = 10 mTorr). After RIE of Si for a predefined duration, the Au NP masks were removed by gold etchant. Finally, the Si stripes with nanopillars were modified with a PFS monolayer.

Si molds for duplicating PDMS microchannels were fabricated by conventional photolithography and wet etching, and PDMS microchannels were prepared by soft lithography. The LPSs were prepared by compressing PDMS microchannels onto the Si surfaces with micro-nanostructures array. A microfluidic fluidic pressure control system (MFCS and FLOWELL, FLUIGENT) were connected to the inlets of the LPS by a soft poly(tetrafluoroethylene) (PTFE) pipe, and the division value of the MFCS is 0.01 mbar. The liquid inlets of the LPSs were treated with oxygen plasma treatment to eliminate the pressure loss of fluid.

Detection of the blood pressure of rats. 45 of 7-10 weeks old SD rats were purchased from Beijing Huafukang Biological Technology Co. Ltd., and used under protocols approved by Jilin University Laboratory Animal Center. Food was removed 2 h before the detections were conducted, and the ambient temperature was maintained at 25 °C. The rats were weighed and injected with pentobarbital sodium ($20 \text{ mg}\cdot\text{Kg}^{-1}$) for anesthesia, and 30 of the rats were divided into six groups: control group, $0.2 \text{ mL}\cdot\text{Kg}^{-1}$ 0.01% adrenaline intravenous injected group, $0.2 \text{ mL}\cdot\text{Kg}^{-1}$ 0.01% acetyl choline intravenous injected group, and the other three groups for detecting the arterial thrombosis model which the common carotid artery of the rats are clipped with low, middle and high pressure, respectively. The detection of systolic blood pressure was conducted by connecting the LPS to the left carotid artery of the rats. The remaining 15 rats were used for the detection of CVP and divided into three groups: untreated group, $2 \text{ mL}\cdot\text{Kg}^{-1}$ 0.9% saline intravenously injected control group, $0.8 \mu\text{g}\cdot\text{Kg}^{-1}$ nitroglycerin intravenously injected group. To detect the CVP of rats, a soft PTFE pipe was inserted into the proximal cerebral end of right external jugular vein of the rats by 3-5 cm (equivalent to the atrial vein) using the venous intubation method, and the other end of the pipe was connected to the LPS. The LPS is kept at the same level as the position of the rat heart during the detection process, and it is necessary to stop bleeding and suture the skin tissue of rats after the measurement process.

Characterization and statistical analysis. Morphologies of the Si-MSNPs structures were characterized by fluorescence microscopy (Olympus BX51 microscope), scanning electron microscopy (JEOLFESEM 6700F electron microscope) and atomic force microscopy (AFM). Dimensions of the microchannels were measured by the Step Profiler (DEKTA 150). Dataphysics OCA20 was performed to measure the surface tension of the fluids and contact angle of the fluids on the surfaces. The flow processes of fluids in the LPS were recorded by an Olympus fluorescence microscope and a smartphone (iPhone 8, Apple). The consumed volume of liquid in the measurement process was calculated according to the dimensions of the

microchannel and the area of filled fluids. All data are expressed as mean \pm standard deviation. Data were compared using an unpaired t-test. P values of <0.05 were considered statistically significant.

Data availability. The authors declare that all data supporting the findings of this study are available within the paper and its supplementary information files.

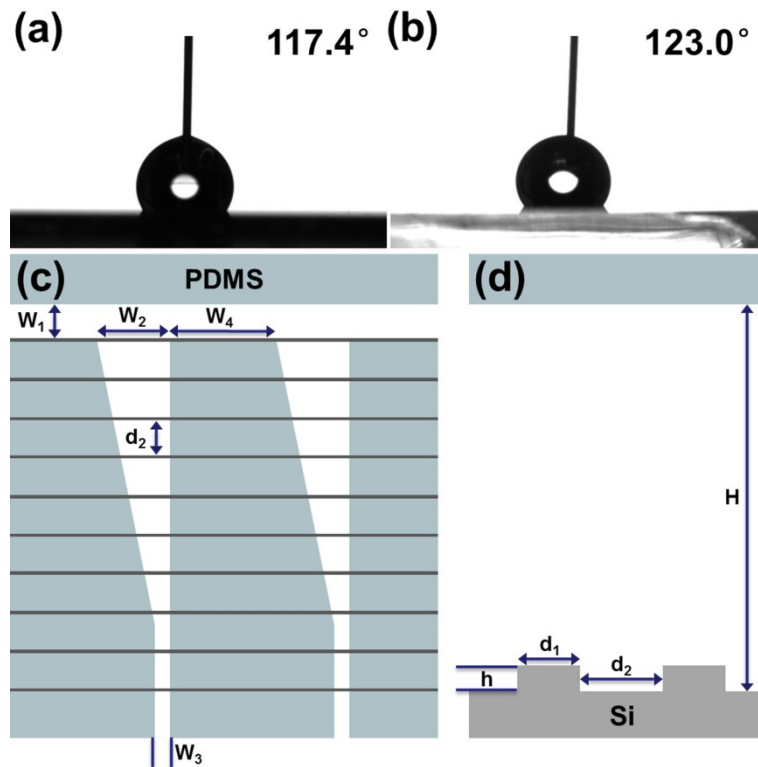


Figure S1. (a) The advancing contact angle of the PFS-modified Si MSNPs surface is $117.4 \pm 0.9^\circ$. (b) The advancing contact angle of the PDMS surface is $123.0 \pm 0.7^\circ$. When liquids flow through the MSNPs, the radius of the gas-liquid-solid three-phase line at the liquid front is greater than its static contact angle due to the Gibbs energy effect. Therefore, we use advancing contact angle to evaluate the Laplace value on liquids in microchannels. (c) Diagram of the LPS, and red lines represent the MSNPs array. $W_1=200 \mu\text{m}$, $W_2=400 \mu\text{m}$, $W_3=40 \mu\text{m}$ and $W_4=800 \mu\text{m}$. (d) Cross-sectional diagram of the LPS. H (the height of the microchannel) $=10 \mu\text{m}$, h (the height of the MSNP) $=1 \mu\text{m}$, d_1 (the width of the MSNP) $=13 \mu\text{m}$, and d_2 (the spacing among the MSNPs) $=70 \mu\text{m}$.

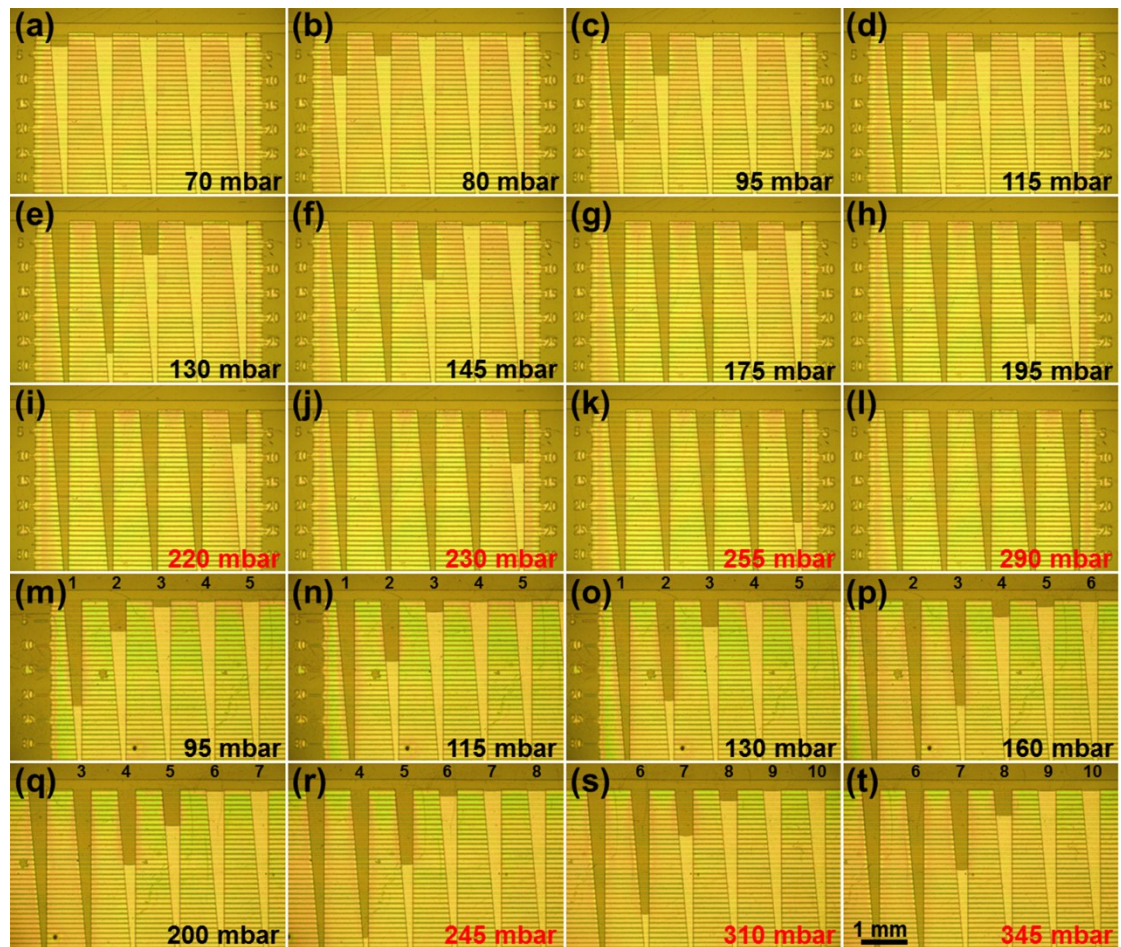


Figure S2. (a-l) Water fills up more grids in the metering microchannels when larger pressure is applied in the liquid inlet. The linear relationship was no longer established when the inlet pressure is larger than 197.0 mbar. The figures in the images represent the applied pressure of the liquid inlet. (m-t) Water fills up more grids in the infinite metering microchannels when larger pressure is applied in the liquid inlet. When the applied pressure of the liquid inlet is larger than 240.0 mbar, the LPS is no longer accurate, which is because that water flows through the whole metering microchannels, and the inner hydraulic pressure is reduced to drive the flow of water. The above and nether figures in the images represent the serial number of the metering microchannels and the applied pressure of the liquid inlet, respectively.

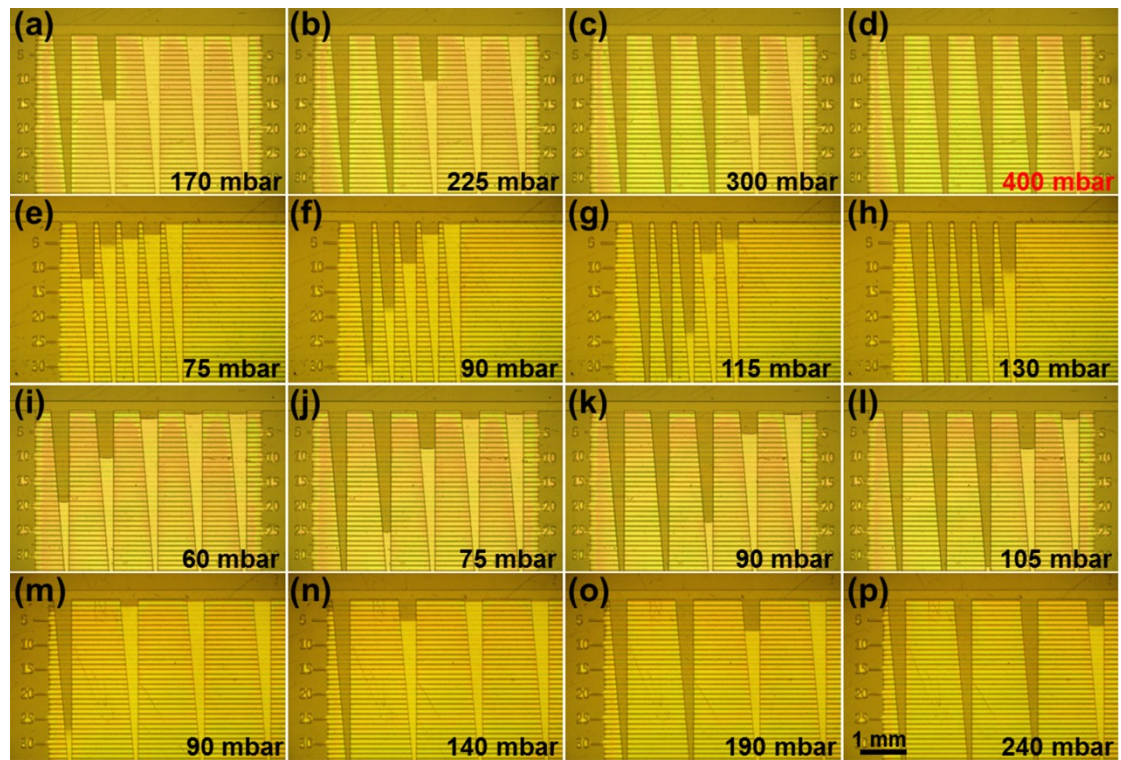


Figure S3. (a-d) The filling behaviors of water in the metering microchannels when the microchannel height of the LPS is 5 μm . (e-h) The filling behaviors of water when the LPS is integrated with distant metering microchannels ($W_4=1600 \mu\text{m}$). The figures in the images represent the applied pressure of the liquid inlet. (i-l) The filling behaviors of water in the metering microchannels when the microchannels heights of the LPS are 30 μm . (m-p) The filling behaviors of water when the LPS is integrated with close metering microchannels ($W_4=200 \mu\text{m}$). The figures in the images represent the applied pressure of the liquid inlet.

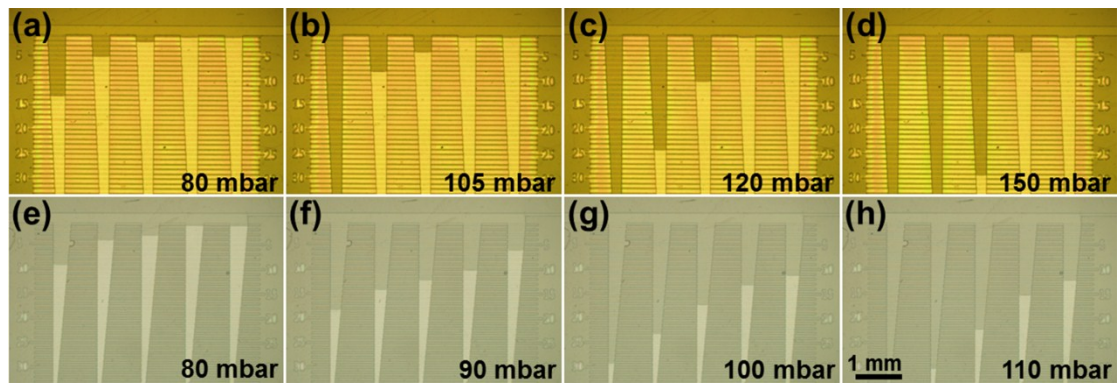


Figure S4. (a-d) The filling behaviors of water in the metering microchannels when the LPS is integrated with wider metering microchannels. The figures in the images represent the applied pressure of the liquid inlet. (e-h) The filling behaviors of water in the metering microchannels when the outlet of the LPS connects a narrow microchannel (Width=40 μm). The figures in the images represent the applied pressure of the liquid inlet.

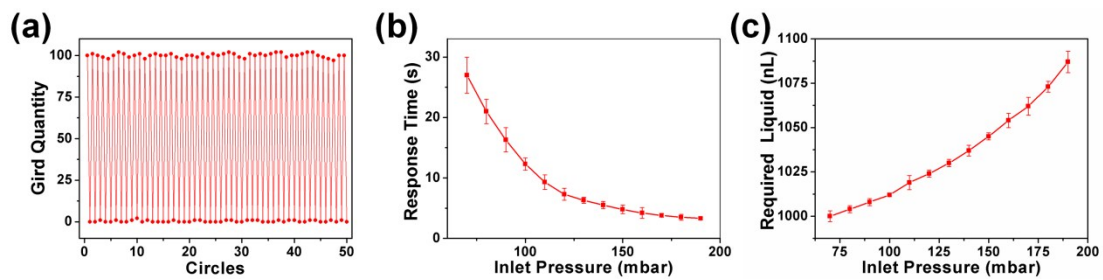


Figure S5. (a) Stability of the LPS. (b) The response time reduces with the increase of the measured pressure. The height of the metering microchannels is 10 μm . (c) The required volume of liquid during the metering process increases with the enlargement of the measured pressure. The height of the metering microchannels is 10 μm .

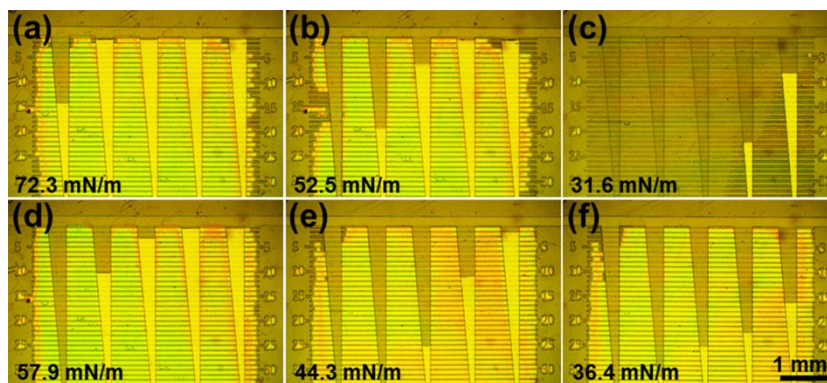


Figure S6. The LPS for sensing the applied pressure of wide surface tension ranges and multiphase liquids, and the applied pressure of liquid inlet is 90.0 mbar. (a) The control liquid is water (surface tension =72.3 mN/m). The measured liquids are (b) BSA solution (surface tension =52.5 mN/m), (c) rapeseed oil (surface tension =31.6mN/m), (d) 5% ethanol (surface tension =57.9 mN/m), (e) 15% ethanol (surface tension =44.3mN/m), and (f) 30% ethanol (surface tension =36.4mN/m), respectively.

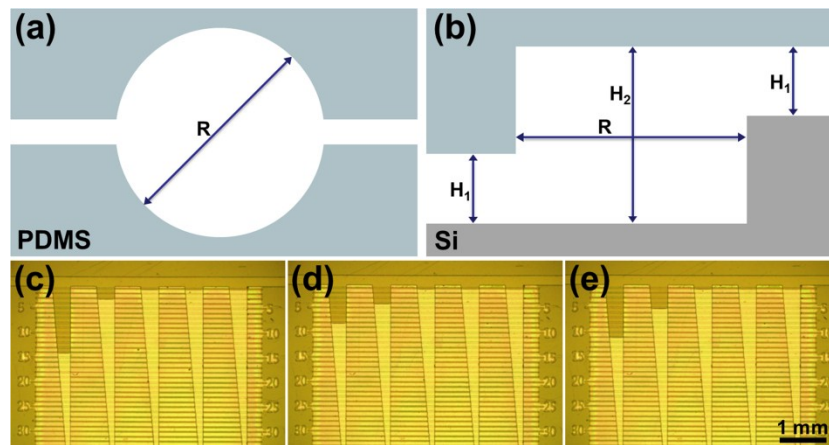


Figure S7. (a) The diagram of the reservoir. The basal diameter of the reservoir is 1 mm (R). (b) Cross-sectional diagram of the LPS, $H_1=10\ \mu\text{m}$, $H_2=100\ \mu\text{m}$. (c-e) A reservoir integrated LPS for sensing the applied pressure of liquids with extremely low surface tension, and the applied pressure of liquid inlet is 90.0 mbar. The measured liquids are (c) ethanol (surface tension =22.1 mN/m), (d) n-hexadecane (surface tension =25.2 mN/m) and (e) octadecene (surface tension =22.0 mN/m), respectively.

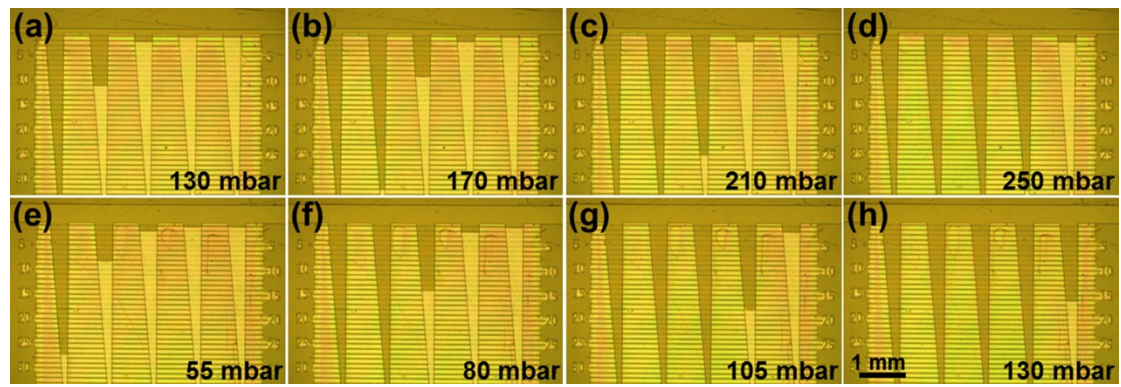


Figure S8. The filling behaviors of water in the metering microchannels when the widths of the fluidic microchannels are 100 μm (a-d) and 300 μm (e-h), respectively. The figures in the images represent the applied pressure of the liquid inlet.

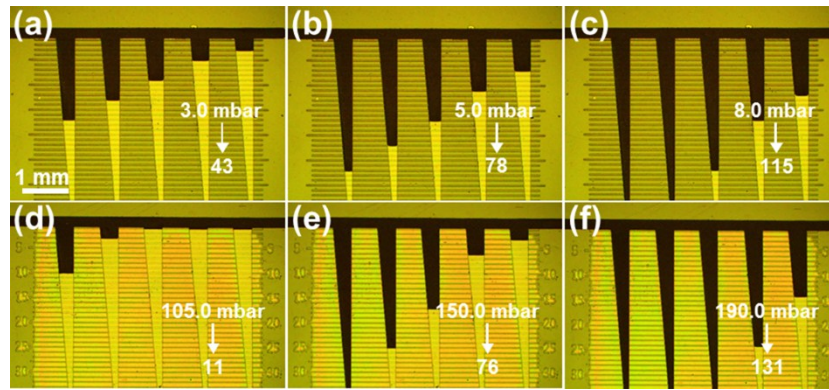


Figure S9. (a-c) Optical microscopy images of the LPS for sensing the simulative central venous pressure. The inlet pressures of the blood chamber are 3.0 (a), 5.0 (b) and 8.0 (c) mbar, respectively. (d-f) Optical microscopy images of the LPS for sensing the simulative systolic blood pressure. The inlet pressures of the blood chamber are 105.0 (d), 150.0 (e) and 190.0 (f) mbar, respectively.

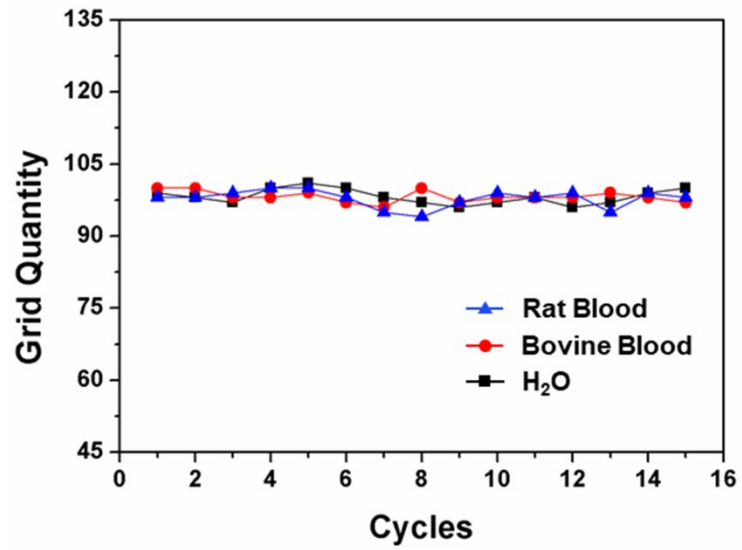


Figure S10. Repeatabilitis of the pressure measurement of H₂O, rat and bovine blood by the LPS. The inlet pressure is 70 mbar, and the microchannel height of the LPS is 83 μm .